Proceeding of the IEEE
International Conference on Robotics and Biomimetics
Dali, China, December 2019

Optimization Design of Redundant Cable Driven Parallel Robots Based on Constant Stiffness Space*

Zhiwei Cui, Xiaoqiang Tang, Senhao Hou, Haining Sun
Department of Mechanical Engineering
Tsinghua University
Beijing, China
{czw16@mails & tang-xq@mail}.tsinghua.edu.cn

Dianjun Wang
Mechanical Engineering Academy
Beijing Institute of Petrochemical Technology
Beijing, China
wangdianjun@bipt.edu.cn

***Abstract* -Cable drive parallel robots (CDPRs) have a flexible structure, highly modular, and are easy to achieve rapid reorganization. To quickly recombine a high-performance CDPRs, the dimension and shape of fixed platform and end-effector is optimized with the maximum constant stiffness space (CSS) volume as the performance index in this paper. Firstly, the static model of CDPRs is established by utilizing the static equilibrium equation, and then the stiffness model and cable tension feasible region previously studied by the author are reviewed. On this basis, the concept and calculation method of the CSS of CDPRs are proposed. Then, the mutual coupling relationship between multiple optimization parameters and their influence on the optimization objective are considered comprehensively. The response surface optimization model is constructed for establishing the relationship between various optimization parameters and optimization objective, and it is solved using sample points selected by utilizing Latin hypercube design method. Finally, the influence of each optimization parameter on the CSS volume is analyzed through the response surface model, and the final optimization result is given.**

Index Terms - Cable Driven Parallel Robots, Optimization Design, Constant Stiffness Space, Response Surface.

I. INTRODUCTION

Cable driven parallel robots (CDPRs) are an extremely important type of industrial robots, and their configurations are very similar to parallel mechanisms. These robots' end-effector is usually driven by utilizing cables substituted rigid links[1-2]. CDPRs have been extensively studied and highly favoured in industrial and academic fields owing to its large workspace, high load capacity, and excellent movement performance[3-6], etc. Therefore, CDPRs have attracted increasing interest for numerous applications such as search and rescue applications[7-9] and rehabilitation[10-14]. The shape and dimension of fixed platform and end-effector have a great influence on the CDPRs' performance. Therefore, under the condition that CDPRs possess the better performance, the shape and dimension optimization of CDPRs is important for achieving rapid reorganization and structural adjustment.

However, CDPRs have also some deficiency. Redundant actuation is required for completely restraint CDPRs owing to driving cables can pull but not push, i.e., to completely control robots with n degrees of freedom (n-DOF CDPRs), at least n + 1 driving cables are required. The n-DOF CDPRs can be also completely controlled via utilizing n cables, if gravity can be seen as equivalent to an additional virtual cable[15]. In different types of CDPRs, the redundant robots usually have more driving cables than their end-effectors' DOFs, and their degree of redundancy (DOR) can be calculation via r = m – n, here m denotes the numbers of actuators[4]. According to the CDPRs performance, several types of workspaces are defined, such as wrench-closure workspace, force-closure workspace, and so on. In [16-17], the concept of wrench-closure workspace (WCW) was introduced, and presented the calculation method of WCW, which can provide a reference for robot's configuration optimization. Barrette and Gosselin [18] defined a new notion of dynamic workspace, and found its shape depends on the accelerations of the end-effector. Pham and Yeo [19] introduced the concept of force-closure workspace and proposed corresponding calculation methods. Arsenault [20] used wrench-closure workspace as the optimization index for optimizing the geometric configuration of CDPRs. In [21-24], the workspace was used as the optimization index to optimize the configuration, dimension or shape of CDPRs. Jiang and Huang [25] used workspace as the optimization index for dimension optimization design of an under-restrained 6-DOF four-cable-driven parallel manipulator based on least square-support vector regression.

On the surface of Mars, in order to look for a suitable landing site, the spacecraft needs to move in a plane, which has a certain height with respect to the surface of Mars, and the stiffness is constant in the plane. Before launching spacecraft, the ground simulation experiments are usually conducted to ensure safety. For ensuring the validity of ground simulation spacecraft Mars landing experiments, the landing state of spacecraft must be simulated as realistically as possible. Therefore, during the experiments, a spacecraft in the addressing plane requires CDPRs with constant stiffness[26]. To the best of the authors' knowledge, considering the constant stiffness space (CSS) as the optimization index for the dimension and shape optimization of CDPRs has not been investigated so far. Most of the above studies take the workspace as the performance index to optimize the configuration, dimension or shape of CDPRs,

* This research work was partially supported by the Beijing Natural Science Foundation and National Natural Science Foundation of China (L182041, No.91648107).

978-1-7281-6321-5/19//$31.00 ©2019 IEEE

which has become more mature methods. However, most of their optimization parameters values usually cannot be continuously changed (such as the number of cables). For the parameters whose values can be continuously changed, the idea of "first sampling and then optimization" is also often adopted, and the study of mathematical model between the optimization variables and performance index is lacking, and coupling relationship between optimization variables is ignored. Response Surface Methods (RSM) [27] is a mature multi-parameter optimization method, which uses approximate mathematical models to describe the interaction between optimization variables and their influence on optimization goal, and has been widely used in research and engineering design. Therefore, this work uses the CSS as the performance index for constructing the response surface model, which can reflect the relationship between various optimization parameters and optimization goal, and optimizes the dimension and shape of CDPRs by comprehensively considering the mutual influence of optimization parameters.

II. Static Model

Diagram of a general CDPR model is described in Fig. 1. CDPR's moving coordinate system O_e and base coordinate system O are assigned, here E_i and F_i are connection points between the cable and end-effector, and the fixed exit point of cables, respectively. Through using the above two coordinate systems, end-effector's position can be depicted by the position vector, $\boldsymbol{p}=[x_{O_e},y_{O_e},z_{O_e}]^{\mathrm{T}}$ (in meters), of the origin of O_e in O and posture can be depicted by the angular displacement, $\boldsymbol{\Theta}=[\alpha,\beta,\gamma]^{\mathrm{T}}$ (in degrees), of O_e relative to O. Thus, $\boldsymbol{x}=[\boldsymbol{p};\boldsymbol{\Theta}]$ represents end-effector's pose in O. Because the size of CDPRs studied in this paper is small, cables' gravity can be neglected, and each cable is regarded as a straight line in the static balance.

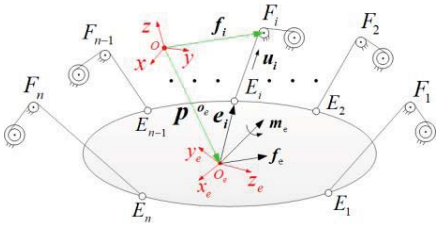

Fig. 1 General model of CDPRs.

According to the static equilibrium condition of CDPRs' end-effector, the static equation can be obtained as follows:

$$\begin{cases}\sum_{i=1}^{m}\mathbf{t}_i+\boldsymbol{f}_e=0\\ \sum_{i=1}^{m}\mathbf{e}_i\times\mathbf{t}_i+\boldsymbol{m}_e=0\end{cases}\tag{1}$$

where $\mathbf{t}_i$ denotes the cable tension of the i^{th} cable, $\overrightarrow{E_iF_i}$ denotes the direction of $\mathbf{t}_i$, $\mathbf{e}_i$ represents vector $\overrightarrow{O_eE_i}$, $\boldsymbol{f}_e$ and $\boldsymbol{m}_e$ denote the resultant force (N) and torque ($\mathrm{N\cdot m}$) (including the gravity of end-effector) of the external force acting on robots, respectively. Let t_i denotes the magnitude of $\mathbf{t}_i$, $\boldsymbol{u}_i$ represents cable unit vector and is the same direction as $\mathbf{t}_i$. Moreover, $\boldsymbol{u}_i$ can be formulated by $\dfrac{\boldsymbol{OF}_i-\boldsymbol{OO}_e-\boldsymbol{O}_e\boldsymbol{E}_i}{\left|\boldsymbol{OF}_i-\boldsymbol{OO}_e-\boldsymbol{O}_e\boldsymbol{E}_i\right|}=\dfrac{\boldsymbol{f}_i-\boldsymbol{p}-\boldsymbol{R}\cdot{}^{o_e}\boldsymbol{e}_i}{\left|\boldsymbol{f}_i-\boldsymbol{p}-\boldsymbol{R}\cdot{}^{o_e}\boldsymbol{e}_i\right|}$, here $\boldsymbol{f}_i$ represents the position vector of F_i in O, ${}^{o_e}\boldsymbol{e}_i$ denotes the position vector of E_i in O_e, $\boldsymbol{R}$ is the rotation matrix of O_e relative to O, and $i=1,2,\cdots,m$.

From (1), the expression of matrix form is given as follows:

$$\boldsymbol{S}\boldsymbol{T}+\boldsymbol{W}=0\tag{2}$$

where $\boldsymbol{T}=\left[t_1,t_2,\cdots,t_m\right]^{\mathrm{T}}$ denotes the cable tension vector, $\boldsymbol{W}=\left[\boldsymbol{f}_{\mathrm{e}},\boldsymbol{m}_{\mathrm{e}}\right]^{\mathrm{T}}$, $\boldsymbol{S}\in\mathrm{R}^{n\times m}$ is the structure matrix of CDPRs at a pose; where

$$\boldsymbol{S}(\boldsymbol{x})=\begin{bmatrix}\boldsymbol{u}_1 & \cdots & \boldsymbol{u}_m\\ (\boldsymbol{R}\cdot{}^{O_e}\boldsymbol{e}_1)\times\boldsymbol{u}_1 & \cdots & (\boldsymbol{R}\cdot{}^{O_e}\boldsymbol{e}_m)\times\boldsymbol{u}_m\end{bmatrix}.$$

III. Analysis of Constant Stiffness Space

Before analysing the CSS of CDPRs, a brief review for stiffness model and cable tension feasible region (CTFR) is as follows [2, 4]:

A. Stiffness Model

The relationship between the small variation $\delta\boldsymbol{x}$ of CDPRs' pose and the small external force $\delta\boldsymbol{W}$ acting on robots can be obtained as follows:

$$\delta\boldsymbol{W}=\boldsymbol{K}\cdot\delta\boldsymbol{x}\tag{3}$$

where $\boldsymbol{K}$ is CDPRs' stiffness matrix.

From (2) and (3), the stiffness matrix can be written by

$$\boldsymbol{K}=\frac{\partial\boldsymbol{W}}{\partial\boldsymbol{x}}=-\left(\frac{\partial\boldsymbol{S}}{\partial\boldsymbol{x}}\boldsymbol{T}+\boldsymbol{S}\frac{\partial\boldsymbol{T}}{\partial\boldsymbol{x}}\right)=\boldsymbol{K}_1+\boldsymbol{K}_2\tag{4}$$

As can be described from (4), the stiffness matrix of CDPRs consists of two parts: $\boldsymbol{K}_1$ is related to the cable tension and structure matrix transformation. It can be controlled via utilizing the tension of driving cables, and is called the controllable stiffness. $\boldsymbol{K}_2$ is related to robots' pose and system structure. It is called the inherent stiffness.

The controllable stiffness of CDPRs is the core to controlling the system stiffness and enabling CDPRs to obtain CSS. From (4), $\boldsymbol{K}_1$ is written as follows:

$$\boldsymbol{K}_1=-\boldsymbol{H}\boldsymbol{T}\tag{5}$$

where $\boldsymbol{H}=\left[\boldsymbol{H}^1,\boldsymbol{H}^2,\cdots,\boldsymbol{H}^n\right]\in\mathrm{R}^{n\times n\times m}$ is the three-dimensional Hessian matrix, $\boldsymbol{H}^j\in\mathrm{R}^{n\times m}$ represents the jth subarray of $\boldsymbol{H}$, and

$$\boldsymbol{H}^j=\frac{\partial\boldsymbol{J}}{\partial\boldsymbol{x}_j}=\begin{bmatrix}\dfrac{\partial\boldsymbol{u}_1}{\partial\boldsymbol{x}_j} & \cdots & \dfrac{\partial\boldsymbol{u}_m}{\partial\boldsymbol{x}_j}\\ \dfrac{\partial\left[(\boldsymbol{R}\cdot{}^{O_e}\boldsymbol{e}_1)\times\boldsymbol{u}_1\right]}{\partial\boldsymbol{x}_j} & \cdots & \dfrac{\partial\left[(\boldsymbol{R}\cdot{}^{O_e}\boldsymbol{e}_m)\times\boldsymbol{u}_m\right]}{\partial\boldsymbol{x}_j}\end{bmatrix}\tag{6}$$

Although the inherent stiffness of CDPRs is not controlled by utilizing tension of driving cables, it still has a significant impact on CDPRs' system stiffness. Using (4), $\boldsymbol{K}_2$ can be obtained as follows:

$$\boldsymbol{K}_2 = -\boldsymbol{S}\frac{\partial \boldsymbol{T}}{\partial \boldsymbol{l}}\frac{\partial \boldsymbol{l}}{\partial \boldsymbol{x}} = \boldsymbol{S}\cdot diag(\frac{\mathrm{E}_1\cdot \mathrm{A}_1}{l_{\mathrm{o1}}},\cdots,\frac{\mathrm{E}_m\cdot \mathrm{A}_m}{l_{\mathrm{om}}})\cdot \boldsymbol{S}^T \quad (7)$$

where E_i, A_i, and l_{oi} represent cables' elastic modulus, cross-sectional area, and static length, respectively.

Controllable stiffness $\boldsymbol{K}_1$ and inherent stiffness $\boldsymbol{K}_2$ can be obtained via utilizing the abovementioned equations, respectively, and CDPRs' stiffness $\boldsymbol{K}$ can be obtained.

B. Cable Tension Feasible Region

From Section II.A, it can be concluded that CDPRs' controllable stiffness can be controlled via utilizing the cable tensions. Therefore, this work investigates CDPRs' CSS based on CTFR. A 2-DOR CDPRs was as research example, when the end-effector's external load is constant, the CTFR can be obtained while preventing cable overload or slack, and satisfying system balance.

Because this work is dedicated to the CSS for 2-DOR CDPRs, when $\boldsymbol{S}$ is a full-rank matrix, (3) can be written as follows:

$$\boldsymbol{T} = \boldsymbol{S}^{+}(-\boldsymbol{W}) + \boldsymbol{N}\boldsymbol{\varphi} = \boldsymbol{t}_p + \boldsymbol{t}_n \quad (8)$$

where $\boldsymbol{S}^{+} = \boldsymbol{S}^{\mathrm{T}}(\boldsymbol{S}\boldsymbol{S}^{\mathrm{T}})^{-1}$ denotes the pseudo-inverse matrix of $\boldsymbol{S}$, $\boldsymbol{N} = \mathrm{null}(\boldsymbol{S})$ is a full-rank $m\times 2$ matrix, $\boldsymbol{\varphi}=[\varphi_1\ \varphi_2]^{\mathrm{T}}$ denotes an 2D vector which represents a point in the plane, $\varphi_1 \in \mathrm{R}$, $\varphi_2 \in \mathrm{R}$, $\boldsymbol{S}^{+}(-\boldsymbol{W})$ denotes the minimum-norm solution of (2) and $\boldsymbol{N}\boldsymbol{\varphi}$ denotes the homogeneous general solution of (2), $\boldsymbol{t}_p = \boldsymbol{S}^{+}(-\boldsymbol{W})$, and $\boldsymbol{t}_n = \boldsymbol{N}\boldsymbol{\varphi}$.

Let $\boldsymbol{\phi}$ denotes the set of tension solutions, $\boldsymbol{T}$, to (2) satisfying the inequalities $t_{\min} \le t_i \le t_{\max}$ defined by the following set of 2m linear inequalities:

$$\mathrm{t}_{\min} - \boldsymbol{t}_p \le \boldsymbol{N}_{m\times 2}\boldsymbol{\varphi} \le \mathrm{t}_{\max} - \boldsymbol{t}_p \quad (9)$$

where $t_{\min}$ and $t_{\max}$ represent the cable-tensions' minimum and maximum limiting values, respectively. Each inequality can define a half plane through a boundary line with $\boldsymbol{\varphi}$ changes, when $t_{\min}$ and $t_{\max}$ are determined. The intersection of 2m half-planes obtained by (9) can form a closed region, and it is referred to as CTFR.

C. Constant Stiffness Space

In practical applications, CDPRs need to meet the system balance, and have a constant stiffness in the working space. For example, the spacecraft landing addressing ground simulation experimental platform system is required to have a constant stiffness in the working plane. The **constant stiffness space** (CSS) of CDPRs is the closed area with constant stiffness, which is formed by the set of poses whose tension of driving cables in the CTFR, and it can be expressed as follows[26]:

$$\text{find} \quad \mathrm{V(x)} \quad (10a)$$

$$\text{subject to} \quad \mathrm{K}(\mathrm{x}_i) = \mathrm{k}_c,\ \boldsymbol{\varphi}_x \in \mathrm{CTFR}(\mathrm{x}_i) \quad (10b)$$

where, x denotes the poses' set, V(x) represents the CSS, x_i represents any pose in the set x, $\mathrm{K}(\mathrm{x}_i)$ represents the CDPRs' system stiffness at pose x_i, k_c denotes a constant matrix, $\boldsymbol{\varphi}_x$ represents an arbitrary point in the plane of $\mathrm{CTFR}(\mathrm{x}_i)$, $\mathrm{CTFR}(\mathrm{x}_i)$ is the robots' CTFR at the pose x_i.

To effectively and quickly determine the CDPRs' CSS, a calculation method is introduced based on the CTFR[26]. The CSS's calculation process and example are described in Fig. 2 and Fig. 3, respectively.

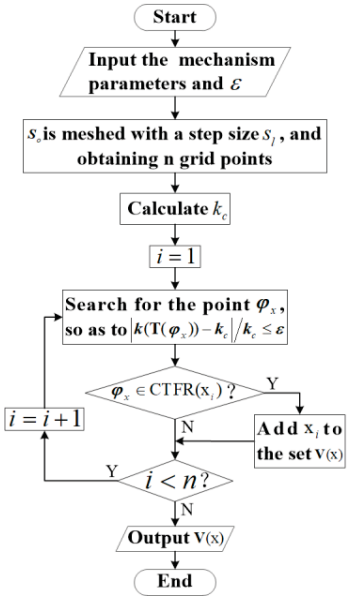

Fig. 2 Flowchart of the CSS algorithm.

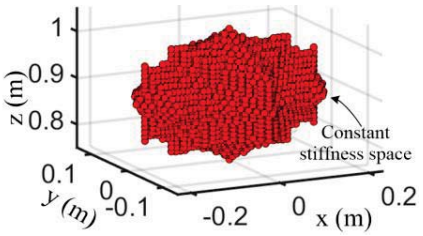

Fig. 3 The instance of the CSS.

IV. Optimization of Dimension and Shape

A. Optimization Model

Because CDPRs can be quickly reconfigured through modular design, and its mechanical structure can also be quickly adjusted to meet different work requirements, it is necessary to research the influence of the different CDPRs' size configurations on the CSS volume. Since the end-effector of CDPRs is non-point-mass in practical applications, the cable tension of driving cables usually generates extra torque to the end-effector. Using (2), $\boldsymbol{W}_c$ can be expressed as follows:

$$\boldsymbol{W}_c = \boldsymbol{S}\boldsymbol{T}=\begin{bmatrix} \boldsymbol{u}_1 & \cdots & \boldsymbol{u}_m \\ e_1\cdot\sin\theta_1\cdot\boldsymbol{\delta}_1 & \cdots & e_m\cdot\sin\theta_m\cdot\boldsymbol{\delta}_m \end{bmatrix}\left[t_1,t_2,\cdots,t_m\right]^{\mathrm{T}} \quad (11)$$

where $\boldsymbol{W}_c=\left[\boldsymbol{f}_c,\boldsymbol{m}_c\right]^{\mathrm{T}}$, $\boldsymbol{f}_c$ and $\boldsymbol{m}_c$ are the resultant force (N) and torque ($\mathrm{N}\cdot\mathrm{m}$) acting on the end-effector of the cable tension of driving-cables, respectively. θ_i denotes the angle between $\mathbf{e}_i$ and $\boldsymbol{u}_i$, $\boldsymbol{\delta}_i$ denotes the unit vector of $(\boldsymbol{R}\cdot{}^{O_e}\boldsymbol{e}_i)\times\boldsymbol{u}_i$.

The results from (11) indicate that the torque of driving-cables' cable tension acting on the end-effector is related with end-effector's pose (pose of end-effector is determined according to the actual operation requirements, and it is fixed) and shape, and is also related to the force arm e_i of the cable tension. $t_i\cdot e_i\cdot\sin\theta_i$ increases along with e_i. The cable tension of driving cables at a certain pose satisfies $\mathrm{t}_{\min}\le\mathrm{t}_i\le\mathrm{t}_{\max}$, which is a necessary and insufficient condition for the pose belong to the CSS. If e_i is very large, then $t_i\cdot e_i\cdot\sin\theta_i$ would be too large that the end-effector cannot generate small moment. Otherwise, if e_i is too small, then the end-effector cannot generate large moment. Therefore, it is important to improve the volume of CSS by optimizing the dimension and shape of CDPRs' end-effector.

Many spatially 6-DOF CDPRs use eight driving cables for redundant driving, and their configuration usually adopts 4-4 configuration, that is, their cable layout is carried out in a symmetrical way, as shown in Fig. 4, both fixed platform and end-effector are cubes. Working space and many other properties of this kind of CDPRs is often symmetry, because their mechanical structure is symmetry, and many scholars have also conducted related research on such CDPRs. Moreover, this kind of CDPRs is also often employed for avoiding the singular configuration. Thus the dimension and shape of the kind of CDPRs is optimized in this paper.

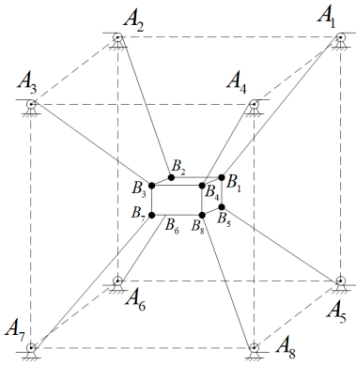

Fig. 4 Spatially 6-DOF CDPRs with eight cables.

This work considers the CSS volume of CDPRs as the optimization target to optimize dimension and shape of CDPRs. The shape and dimension of the fixed frame and end-effector have a great influence on the volume of CSS, and there is a certain proportional relationship between the dimensions. The ratio between any two structural sizes of CDPRs is called the dimension proportionality coefficient (DPC). The influence of different DPCs on the performance of CDPRs is coupled with each other. The result obtained by simple superposition of single optimal parameters, which is obtained by the optimization method of control variables, is usually not the global optimal result. Therefore, this study comprehensively considers the influence of all DPCs on the CDPRs' CSS volume to optimize the dimension and shape of CDPRs. Assume V represents the CDPRs' CSS volume, the expression can be written as follows:

$$V = f(\eta_1,\eta_2,\eta_3,\eta_4,\eta_5) \quad (12)$$

where, $\eta_1=\mathrm{L}_b/\mathrm{L}_e,\eta_2=\mathrm{W}_b/\mathrm{W}_e,\eta_3=\mathrm{H}_b/\mathrm{H}_e,\eta_4=\mathrm{L}_b/\mathrm{W}_b,\eta_5=\mathrm{L}_b/\mathrm{H}_b$, $\eta_i(i=1,2,\cdots,5)$ represent DPC; $\mathrm{L}_e(\mathrm{B}_1\mathrm{B}_2)$, $\mathrm{W}_e(\mathrm{B}_2\mathrm{B}_3)$ and $\mathrm{H}_e(\mathrm{B}_2\mathrm{B}_6)$ denote the length, width and height of the cube formed by connection points between the end-effector and cables, respectively; $\mathrm{L}_b(\mathrm{A}_1\mathrm{A}_2)$, $\mathrm{W}_b(\mathrm{A}_2\mathrm{A}_3)$ and $\mathrm{H}_b(\mathrm{A}_2\mathrm{A}_6)$ represent the length, width and height of the cube formed by the cables' fixed exit points, respectively. Moreover, the position of the cables' fixed exit points on the fixed platform and the connection points between the cables and end-effector can be arbitrarily changed to obtain an optimum shape and dimension for an already designed CDPR. Therefore, when optimizing an already designed CDPR, it is not necessary to change the shape and dimension of the fixed frame. After the DPCs of CDPRs are determined, the dimension of CDPRs can be determined by determining arbitrarily a structural size.

This study gives the limited size, H_b ($\mathrm{H}_b=1.78\,\mathrm{m}$), of the CDPR, and the dimension and shape of the CDPR is optimized by optimizing the DPCs. Therefore, the following mathematical expression is used to describe the optimization problem of CDPRs in this work:

$$\begin{aligned} &\max && V(\mathrm{x}) \\ &\text{subject to} && \phi_i\le\eta_i\le\vartheta_i \end{aligned} \quad (13)$$

where, $V(\mathrm{x})$ is the volume of CSS, ϕ_i and ϑ_i represent the minimum and maximum limiting values of DPCs.

To comprehensively analyse the influence of all DPCs on the performance of CDPRs, this study uses the response surface method to optimize the DPCs of CDPRs, and then realize the optimization of CDPRs' dimension and shape.

Meanwhile, this work uses the quadratic polynomial as the response surface function model to make the response surface function reflect the actual function without being too complicated, and its expression is as follows:

$$V_p(\mathrm{x}) = \mu_0 + \sum_{i=1}^{n}\mu_i x_i + \sum_{k=1}^{n}\sum_{i=k}^{n}\mu_{ki}x_k x_i \quad (14)$$

where, $V_p(\mathrm{x})$ represents the predicted response value of the CSS volume of CDPRs, x_i represents the i^{th} component of the n dimensional independent variable, μ_0, μ_i and μ_{ki} denote the coefficient of the polynomial, which can be resolved by using least squares method.

B. Experimental Analysis

In order to obtain the ideal response surface model, and then optimize the dimension and shape of CDPRs, the DOE (design of experiments) method is used to determine the coefficient in (14) in this paper. The approximation accuracy of the response surface is largely dependent on the positional distribution of the sample points in the design space. Because there are many parameters to be optimized in this work, and the shape of optimization target is irregular, it is difficult to obtain ideal results utilize the sample points obtained by single Box-Behnken Design and Central Composite Design methods. Fortunately, the number of sample points of the Latin hypercube design method can be artificially set. It adopts the principle of equal probability orthogonal distribution, and can obtain a higher precision response surface equation utilize very few sample points. Therefore, this study uses the Latin hypercube design method to arrange the locations of the sample points. According to the practical engineering requirements, the limiting value of the DPCs shown in Table I is used as the example to optimize the dimension and shape of CDPRs. The CDPR's system stiffness, which is controlled by utilizing the cable tension at the CTFR's centroid, is considered as the CSS's stiffness matrix, when the CDPR's end-effector is at the pose $x=[0,0,\mathrm{H}_b\,(1\text{-}1/20),0,0,0]^{\mathrm{T}}$ and its external load is zero. In this work, the definition domain of design variables is divided into two non-overlapping intervals according to the principle of equal probability, and a number is randomly selected in each interval, and these numbers are randomly combined to form a set of sample points. Another set of sample points is taken from the said interval in the same manner. Deleting the singular points in the two sets of sample points and the remaining points are combined together as sample points, as depicted in Fig. 5.

Table I The limiting values of the DPCs.

Limiting values	η_1	η_2	η_3	η_4	η_5
ϕ	2	2	2	0.2	0.2
ϑ	20	20	20	5	5

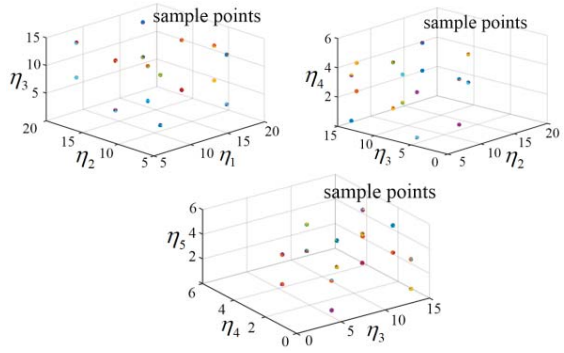

Fig. 5 Sample points are arranged by utilizing Latin hypercube design method.

Using the sample points shown in Fig. 5 fitting to solve (14) by the least squares method, and the expression of second-order polynomial response surface approximation model is as follows:

$$\begin{aligned} V(\mathrm{x}) = & 39.77 + 23.82\eta_1 - 11.73\eta_2 - 17.04\eta_3 - 67.84\eta_4 \\ & + 112.37\eta_5 - 8.20\eta_1\eta_2 - 5.28\eta_1\eta_3 + 37.47\eta_1\eta_4 + 30.79\eta_1\eta_5 \\ & - 29.15\eta_2\eta_3 - 24.09\eta_2\eta_4 - 27.06\eta_2\eta_5 + 9.41\eta_3\eta_4 - 19.05\eta_3\eta_5 \\ & - 120.59\eta_4\eta_5 + 11.72\eta_2^2 + 8.61\eta_3^2 + 151.52\eta_4^2 + 8.54\eta_5^2 \end{aligned} \tag{15}$$

The R-Squared $R^2(0.8825>0.8)$ and Adj R-Squared $R_{adj}^2(0.8238>0.8)$ of the said model are both close to 1, and the values are close, which indicates that this model can be used to evaluate the volume of CSS. Correspondingly, the response surface obtained by utilizing this model is shown in Fig. 6.

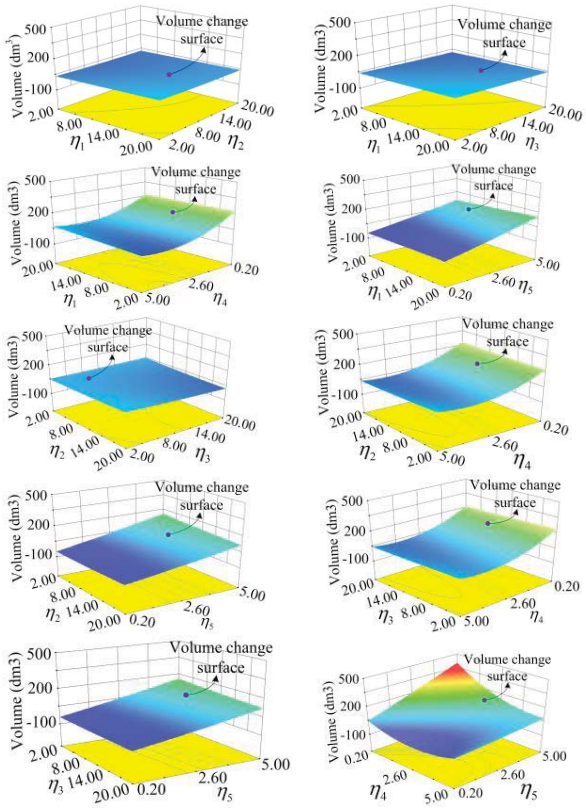

Fig. 6. Response surface model

It can be concluded from Fig. 6 that the change of η_1, η_2 and η_3 has no obvious influence on the CSS volume of CDPRs, when the height of fixed platform is determined ($\mathrm{H}_b=1.78\,\mathrm{m}$). The change of η_4 and η_5 has a great influence on the CSS volume of CDPRs. With the decrease of η_4 and the increase of η_5, the volume of CSS gradually increases.

Therefore, comprehensive considering the influence of multiple DPCs on the CSS volume of CDPRs, and the response surface analysis experimental is used to obtain the optimal DPC and the corresponding CSS volume as shown in Table II.

Table II The optimization results

η_1	η_2	η_3	η_4	η_5	V(dm^3)
11.97	2.86	14.79	0.30	4.86	484.7

V. CONCLUSION

The 6-DOF eight-cable-driven parallel robot is considered as an example in this work. Firstly, the static model of CDPRs is established by utilizing the static equilibrium equation, and then the stiffness model and the CTFR previously studied by the author are reviewed. Then, the concept and calculation method of the CDPRs' CSS are proposed. Finally, the response surface model between the various optimization parameters and the optimization target is constructed by comprehensively considering the mutual coupling relationship between each optimization parameter and its influence on the optimization target. When the height of the fixed platform is limited to 1.78 m, the response surface model is used to optimize CDPRs. It is found that the CSS volume of CDPRs is less affected by η_1, η_2 and η_3, and is greatly influenced by η_4 and η_5, and the volume of CSS gradually increases as η_4 decreases and η_5 increases. The influence of the various DPCs on the CSS volume of CDPRs is considered comprehensively, and the optimal shape and dimension of CDPRs is finally obtained.

The method is illustrated via considering 6-DOF eight-cable-driven parallel robot as an example. Nevertheless, the method is not limited to the optimization of the eight-cable-driven parallel robots, and can also be used for or provide reference for other robots optimization.

REFERENCES

[1] Berti A, Merlet J P, Carricato M. Solving the direct geometrico-static problem of underconstrained cable-driven parallel robots by interval analysis[J]. The International Journal of Robotics Research, 2016, 35(6): 723-739.

[2] Cui Z, Tang X, Hou S, et al. Non-iterative geometric method for cable-tension optimization of cable-driven parallel robots with 2 redundant cables[J]. Mechatronics, 2019, 59: 49-60.

[3] Dion-Gauvin P, Gosselin C. Dynamic Point-to-Point Trajectory Planning of a Three-DOF Cable-Suspended Mechanism Using the Hypocycloid Curve[J]. IEEE/ASME Transactions on Mechatronics, 2018, 23(4): 1964-1972.

[4] Cui Z, Tang X, Hou S, et al. Research on Controllable Stiffness of Redundant Cable-Driven Parallel Robots[J]. IEEE/ASME Transactions on Mechatronics, 2018, 23(5): 2390-2401.

[5] Pott A, Bruckmann T, Mikelsons L. Closed-form force distribution for parallel wire robots[M]//Computational Kinematics. Springer, Berlin, Heidelberg, 2009: 25-34.

[6] Lim W B, Yeo S H, Yang G. Optimization of tension distribution for cable-driven manipulators using tension-level index[J]. IEEE/ASME Transactions on Mechatronics, 2014, 19(2): 676-683.

[7] Bosscher P, Williams R L, Tummino M. A concept for rapidly-deployable cable robot search and rescue systems[C]//ASME 2005 International Design Engineering Technical Conferences and Computers and Information in Engineering Conference. American Society of Mechanical Engineers, 2005: 589-598.

[8] Merlet J P. MARIONET, a family of modular wire-driven parallel robots[M]//Advances in Robot Kinematics: Motion in Man and Machine. Springer, Dordrecht, 2010: 53-61.

[9] Tadokoro S, Verhoeven R, Hiller M, et al. A portable parallel manipulator for search and rescue at large-scale urban earthquakes and an identification algorithm for the installation in unstructured environments[C]//Proceedings 1999 IEEE/RSJ International Conference on Intelligent Robots and Systems. Human and Environment Friendly Robots with High Intelligence and Emotional Quotients (Cat. No. 99CH36289). IEEE, 1999, 2: 1222-1227.

[10] Rosati G, Secoli R, Zanotto D, et al. Planar robotic systems for upper-limb post-stroke rehabilitation[C]//ASME 2008 International Mechanical Engineering Congress and Exposition. American Society of Mechanical Engineers, 2008: 115-124.

[11] Rosati G, Gallina P, Masiero S. Design, implementation and clinical tests of a wire-based robot for neurorehabilitation[J]. IEEE Transactions on Neural Systems and Rehabilitation Engineering, 2007, 15(4): 560-569.

[12] Mao Y, Jin X, Dutta G G, et al. Human movement training with a cable driven arm exoskeleton (CAREX)[J]. IEEE Transactions on Neural Systems and Rehabilitation Engineering, 2015, 23(1): 84-92.

[13] Wang Y, Chen J, Zhu K, et al. Practical Tracking Control of Cable-Driven Robots Using Adaptive Nonsingular Fast Terminal Sliding Mode[J]. IEEE Access, 2018, 6: 68057-68069.

[14] Cui X , Chen W , Jin X , et al. Design of a 7-DOF Cable-driven Arm Exoskeleton (CAREX-7) and a Controller for Dexterous Motion Training or Assistance[J]. IEEE/ASME Transactions on Mechatronics, 2016, 22(1):1-1.

[15] X. Jiang, C. Gosselin, "Trajectory Generation for Three-degree-of-freedom Cable-suspended Parallel Robots Based on Analytical Integration of the Dynamic Equations," Journal of Mechanisms & Robotics, vol. 8, no. 4, 2015.

[16] Azizian K , Cardou P , Moore B . Classifying the Boundaries of the Wrench-Closure Workspace of Planar Parallel Cable-Driven Mechanisms by Visual Inspection[J]. Journal of Mechanisms & Robotics, 2012, 4(2):437-448.

[17] Lau D , Oetomo D , Halgamuge S K . Wrench-Closure Workspace Generation for Cable Driven Parallel Manipulators Using a Hybrid Analytical-Numerical Approach[J]. Journal of Mechanical Design, 2011, 133(7):071004.

[18] Barrette G , Gosselin C M . Determination of the Dynamic Workspace of Cable-Driven Planar Parallel Mechanisms[J]. Journal of Mechanical Design, 2005, 127(2):242.

[19] Pham C B , Yeo S H , Yang G , et al. Force-closure workspace analysis of cable-driven parallel mechanisms[J]. Mechanism & Machine Theory, 2006, 41(1):53-69.

[20] Arsenault M . Optimization of the prestress stable wrench closure workspace of planar parallel three-degree-of-freedom cable-driven mechanisms with four cables[C]// IEEE International Conference on Robotics & Automation. IEEE, 2010.

[21] Bahrami A , Bahrami M N . Comments on "Design and workspace analysis of a 6–6 cable-suspended parallel robot"[J]. Mechanism & Machine Theory, 2016, 98(-):1-1.

[22] Lamine H , Bennour S , Romdhane L . Design of cable-driven parallel manipulators for a specific workspace using interval analysis[J]. Advanced Robotics, 2016:1-10.

[23] FATTAH, Abbas, AGRAWAL, et al. On the design of cable-suspended planar parallel robots[J]. Journal of Mechanical Design, 2005, 127(5):1021-1028.

[24] Hay A M , Snyman J A . Optimization of a planar tendon-driven parallel manipulator for a maximal dextrous workspace[J]. Engineering Optimization, 2005, 37(3):217-236.

[25] Jiang, Huang, Zheng. Dimension optimization design of an under-restrained 6-DOF four-cable-driven parallel manipulator based on least square-support vector regression[C]// International Conference on Mechatronics & Automation. IEEE, 2011.

[26] Cui Z, Tang X, Hou S, et al. Calculation and Analysis of Constant Stiffness Space for Redundant Cable-Driven Parallel Robots[J]. IEEE Access, 2019, 7: 75407-75419.

[27] SUI Yunkang , YU Huiping . Improvement of response surface method and its application to engineering optimization[M] . Beijing : Science Press , 2011.